Near-Field Antenna Measurements Using Nonideal Measurement Locations

Ronald C. Wittmann, *Senior Member, IEEE*, Bradley K. Alpert, and Michael H. Francis, *Senior Member, IEEE*

Abstract—We introduce a near-field to far-field transformation algorithm that relaxes the usual restriction that data points be located on a plane rectangular grid. Computational complexity is $\mathcal{O}(N \log N)$ where N is the number of data points. This algorithm allows efficient processing of near-field data with known probe position errors. Also, the algorithm is applicable to other measurement approaches such as plane-polar scanning, where data are collected intentionally on a nonrectangular grid.

Index Terms—Antenna measurements.

I. INTRODUCTION

WE introduce a near-field to far-field transformation method that relaxes the usual restriction that data points be located on a plane-rectangular grid. It is not always practical or desirable to make uniformly spaced measurements; for example, the maintenance of positioning tolerances becomes more difficult as frequency is increased. Our algorithm allows efficient processing of data with probe position errors. This method can extend the frequency ranges of existing scanners, make practical the use of portable scanners for on-site measurements, and support schemes such as plane-polar scanning, where data are intentionally collected on a nonrectangular grid.

Although "ideal" locations are not required, we assume that probe positions are known. (In practice, laser interferometry is often used for this purpose.) Our approach is based on a linear model of the form $\mathbf{A}\boldsymbol{\xi} = \mathbf{b}$ (see Section II). The conjugate gradient method is used to find the "unknown" $\boldsymbol{\xi}$ in terms of the "data" $\mathbf{b}$ (Section III). The operator $\mathbf{A}$ must be applied once per conjugate gradient iteration and this is done efficiently using the recently developed unequally spaced fast Fourier transform (FFT) [2], [3] and local interpolation (Section IV). As implemented, each iteration requires $\mathcal{O}(N \log N)$ operations, where N is the number of measurements. The required number of iterations depends on desired computational accuracy and on conditioning. In Section V, we present several simulations that are based on actual near-field antenna data.

II. THE MODEL

A. Discrete Theory

Consider a transmitting test antenna and a receiving probe. According to Kerns's theory (see Appendix A), the response

$w(\mathbf{r})$ of a probe located at $\mathbf{r}$ may be modeled as

$$w(\mathbf{r}) = \sum_{\nu\mu} \xi_{\nu\mu} \exp(i\mathbf{k}_{\nu\mu} \cdot \mathbf{r}) \qquad (1)$$

where $\xi_{\nu\mu}$ is the (normalized) coupling product and

$$\mathbf{k}_{\nu\mu} \equiv \frac{\pi\nu}{L_x}\hat{\mathbf{x}} + \frac{\pi\mu}{L_y}\hat{\mathbf{y}} + \gamma_{\nu\mu}\hat{\mathbf{z}}$$

$$\gamma_{\nu\mu} \equiv \sqrt{k^2 - \left(\frac{\pi\nu}{L_x}\right)^2 - \left(\frac{\pi\mu}{L_y}\right)^2}.$$

We assume that the probe response is negligible outside the interval $|x| \leq L_x$, $|y| \leq L_y$ for z values of interest. (That is, $w(\mathbf{r})$ is a periodic extension.) To improve conditioning, *we include only propagating plane waves* ($\gamma_{\nu\mu}$ real) in the summation in (1). Evanescent waves ($\gamma_{\nu\mu}$ imaginary) are exponentially attenuated and are negligible in the far-field region. We must also ensure that evanescent waves are not important contributors to the measured probe response; this is usually accomplished by maintaining a probe-to-test-antenna separation of several wavelengths.

In matrix form (1) becomes

$$\mathbf{w} = \mathbf{Q}\boldsymbol{\xi} \qquad (2)$$

where $\mathbf{w} \equiv \{w(\mathbf{r}_n)\}$, $\mathbf{r}_n$ is the location of the nth measurement point, $\boldsymbol{\xi} \equiv \{\xi_{\nu\mu}\}$, and $\mathbf{Q} \equiv \{Q_{n,\nu\mu} = \exp(i\mathbf{k}_{\nu\mu} \cdot \mathbf{r}_n)\}$. The objective of near-field to far-field transformation is to determine the coupling product $\boldsymbol{\xi}$ from measurements $\mathbf{w}$ made in a restricted region near the test antenna. The transmitting (far-field) pattern can be found from the coupling products of the test antenna with each of two independent known probes.

B. Normal Equations

In practical situations, where the number of measurements often exceeds the number of unknowns, the system (2) is overdetermined and will generally not have a solution. We will actually solve the normal equations

$$\mathbf{A}\boldsymbol{\xi} = \mathbf{b} \qquad (3)$$

where

$$\mathbf{A} \equiv \mathbf{Q}^H \mathbf{Q}$$
$$\mathbf{b} \equiv \mathbf{Q}^H \mathbf{w}. \qquad (4)$$

The operator $\mathbf{Q}^H \equiv \{Q_{\nu\mu,n}^H = \exp(-i\mathbf{k}_{\nu\mu}^* \cdot \mathbf{r}_n)\}$ is the Hermitian (conjugate) transpose of $\mathbf{Q}$. The solution $\boldsymbol{\xi}$ of (3) minimizes $\|\mathbf{w} - \mathbf{Q}\boldsymbol{\xi}\|$; that is, this $\boldsymbol{\xi}$ is the least-squares

estimate. Most methods for processing planar near-field data [based on the model (1)] solve (3), either directly or indirectly. In the standard plane-rectangular grid algorithm, $\mathbf{A}$ is diagonal and $\mathbf{Q}^H$ and $\mathbf{Q}$ can be applied with FFT's, giving a computational complexity of $\mathcal{O}(N \log N)$. On the other hand, a direct solution using Gaussian elimination requires $\mathcal{O}(N^3)$ operations. For typical problem sizes ($10^4 < N < 10^6$), the importance of computational efficiency is readily apparent.

III. CONJUGATE GRADIENT SOLUTION

A. Algorithm

Since $\mathbf{A}$ is Hermitian and positive definite (assuming that $\mathbf{Q}$ is full rank), the conjugate gradient method is applicable (see, for example, [4]). The algorithm is an iterative scheme given by

$$\mathbf{d}^{(0)} = \mathbf{r}^{(0)} = \mathbf{b} - \mathbf{A}\boldsymbol{\xi}^{(0)}$$
$$\chi_j = \frac{\|\mathbf{r}^{(j)}\|^2}{[\mathbf{d}^{(j)}]^H \mathbf{A} \mathbf{d}^{(j)}}$$
$$\boldsymbol{\xi}^{(j+1)} = \boldsymbol{\xi}^{(j)} + \chi_j \mathbf{d}^{(j)} \qquad (5)$$
$$\mathbf{r}^{(j+1)} = \mathbf{r}^{(j)} - \chi_j \mathbf{A} \mathbf{d}^{(j)}$$
$$\mathbf{d}^{(j+1)} = \mathbf{r}^{(j+1)} + \frac{\|\mathbf{r}^{(j+1)}\|^2}{\|\mathbf{r}^{(j)}\|^2} \mathbf{d}^{(j)}$$

where $\|\mathbf{y}\|^2 \equiv \mathbf{y}^H \mathbf{y}$. Initial estimates are not critical and we use $\boldsymbol{\xi}^{(0)} = 0$ for simplicity. Somewhat earlier convergence may be obtained, for example, by starting with the coupling product obtained from k-corrected data [5]. The quantity $\mathbf{r}^{(j)} = \mathbf{b} - \mathbf{A}\boldsymbol{\xi}^{(j)}$ is the jth residual.

B. Conditioning and Convergence

The rate of convergence can be estimated with [6, p. 525]

$$\|\boldsymbol{\xi}^{(j)} - \boldsymbol{\xi}\|_A \leq 2 \left(\frac{c-1}{c+1} \right)^j \|\boldsymbol{\xi}^{(0)} - \boldsymbol{\xi}\|_A \qquad (6)$$

where $\|\mathbf{y}\|_A^2 \equiv \mathbf{y}^H \mathbf{A} \mathbf{y}$ and the condition number c^2 is the ratio of the largest to smallest eigenvalue of $\mathbf{A}$. (The condition number of $\mathbf{Q}$ is c, $c \geq 1$.) Thus, the conjugate gradient algorithm will *always* converge. For each j it minimizes $\|\boldsymbol{\xi}^{(j)} - \boldsymbol{\xi}\|_A$ for $\boldsymbol{\xi}^{(j)} - \boldsymbol{\xi}^{(0)}$ in the Krylov space span $\{\mathbf{r}^{(0)}, \mathbf{A}\mathbf{r}^{(0)}, \cdots, \mathbf{A}^{j-1}\mathbf{r}^{(0)}\}$.

Relative error is bounded by the residual

$$\frac{\|\boldsymbol{\xi}^{(j)} - \boldsymbol{\xi}\|}{\|\boldsymbol{\xi}\|} \leq c^2 \frac{\|\mathbf{r}^{(j)}\|}{\|\mathbf{b}\|}. \qquad (7)$$

If we suppose that "perfect" measurements $\mathbf{w}_0$ and "imperfect" measurements $\mathbf{w}$ correspond to the solutions [of (3)] $\boldsymbol{\xi}_0$ and $\boldsymbol{\xi}$, then

$$\frac{\|\boldsymbol{\xi} - \boldsymbol{\xi}_0\|}{\|\boldsymbol{\xi}_0\|} \leq c \frac{\|\mathbf{w} - \mathbf{w}_0\|}{\|\mathbf{w}_0\|}. \qquad (8)$$

For large condition numbers (poor conditioning), (6)–(8) indicate *potential* problems with convergence rate, computational accuracy, and/or experimental design. Fortunately, it is often possible to improve conditioning by adding physically

reasonable restrictions. For example, arbitrarily large condition numbers can arise when evanescent plane waves are included in the model (1). In the examples of Section V, the exclusion of evanescent fields results in acceptable condition numbers.

When *all* evanescent modes are excluded and data are measured on the regular (ideal) grid (18), the condition number is $c = 1$. On the other hand, substantial values of c can result when data density is significantly nonuniform. In some simulations involving large position errors, projection of the measurement locations onto the xy plane defined a region with scalloped edges. If L_x and L_y were large enough to define a rectangle containing all the data points, the gaps due to the scallops led to poor conditioning. Our solution was to choose slightly smaller values for L_x and L_y and to discard data points lying outside this boundary. Similarly, when there are regions with high data densities (as in plane-polar scanning), condition numbers can often be markedly improved by thinning or otherwise weighting data points consistent with a uniform "information density." To find a weighted least-squares estimate, replace (4) with

$$\mathbf{A} \equiv \mathbf{Q}^H \kappa \mathbf{Q}$$
$$\mathbf{b} \equiv \mathbf{Q}^H \kappa \mathbf{w} \qquad (9)$$

where κ is a diagonal matrix. In particular, κ_{nn} is a positive weight to be associated with the measurement point $\mathbf{r}_n$.

It is tempting to consider the possibility of choosing L_x and L_y to encompass a region much larger than the actual measurement area. This would mitigate truncation effects (since the probe response is not implicitly assumed to be zero immediately beyond the measurement region) and would seem to allow determination of the sidelobes from measurements made near the main-beam zone. In practice, such a model quickly becomes useless because of poor conditioning. Schemes which produce wide-angle pattern coverage from limited measurement data must invariably rely on *a priori* information about the antenna under test [7]–[9].

IV. EFFICIENCY

In the conjugate gradient procedure of (5), it is necessary to apply the matrix $\mathbf{A} = \mathbf{Q}^H \mathbf{Q}$ to a vector once each iteration. This can be done by a straightforward summation, but only in $\mathcal{O}(N^2)$ operations. In order to reduce complexity to $\mathcal{O}(N \log N)$ operations per iteration, we have developed a scheme that combines the unequally spaced FFT with interpolation in z. For example, to apply $\mathbf{Q}$ to $\boldsymbol{\xi}^{(j)}$ we use the unequally spaced FFT to evaluate (2) (in $\mathcal{O}(N \log N)$ operations) at the points $x_n \hat{\mathbf{x}} + y_n \hat{\mathbf{y}} + z \hat{\mathbf{z}}$ for several fixed values of z. We then use local interpolation in z to reach the actual measurement locations $\mathbf{r}_n$. Since we are dealing with bandlimited functions, the numerical precision of the algorithm can be controlled and is specified as an input parameter. Computational time depends on the desired numerical accuracy and on the spatial distribution of data points. Our technique is most efficient when measurement locations lie close to a plane. Details are given in Appendix B.
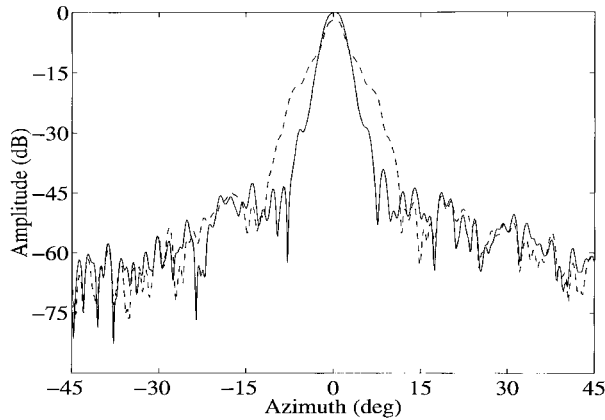
Fig. 1. H-plane far-field pattern of the radiometer. Probe position errors are given by (10). The solid line corresponds to the corrected pattern and to the actual pattern. The dashed line shows the result of ignoring the position errors.

Fig. 2. H-plane far-field pattern of the radiometer. Probe position errors are given by (11). The solid line corresponds to the corrected pattern and to the actual pattern. The dashed line shows the result of ignoring the position errors.

V. SIMULATIONS

A. Probe Position Errors

We began with planar near-field data for a radiometer antenna with an aperture diameter of 25 cm and an operating frequency of 31.65 GHz. These data consist of 161 points in x by 161 points in y on an ideal grid spaced by 0.38 cm (0.4λ). The model (1) was specified with $L_x = L_y = 161 \times 0.38/2 = 30.59$ cm and the coupling product was calculated using standard near-field to far-field transformation software. Position errors were then simulated by using (1) to calculate the probe response at nonideal measurement locations. In this setup, there are about 26 000 simulated measurements and about 20 000 unknowns (evanescent modes excluded). We present five cases.

For the first case, we used a moderate position error of the form

$$
\begin{pmatrix} \delta x \\ \delta y \\ \delta z \end{pmatrix} = \begin{pmatrix} 0.14 \cos(0.35n) \cos(0.65m) \\ 0.14 \cos(0.25n) \cos(0.15m) \\ 0.20 \cos(0.15n) \cos(0.11m) \end{pmatrix} \lambda \quad (10)
$$

where n is the x index and m is the y index. Both indexes run from -80 to $+80$. Peak magnitude of this position error is 0.28λ and the rms magnitude is 0.14λ. Fig. 1 shows the result of probe position correction in this example. There is no discernible difference between actual and position corrected patterns, as expected from (7). The pattern computed ignoring probe position errors, however, has a broader main beam and also has a gain that is about 2 dB low. The relative residual at the jth iteration is defined as

$$
\tau_j \equiv \|\mathbf{r}^{(j)}\| / \|\mathbf{b}\|.
$$

We terminate our program after $j_{\max}$ iterations or after the relative residual becomes less than τ (say, $j_{\max} = 100$ and $\tau = 10^{-8}$). For the displacements (10), the condition number is $c^2 \approx 13$, $\tau_5 < 10^{-4}$, and $\tau_{19} < 10^{-8}$. Condition numbers are estimated using a procedure due to Lanczos [6, p. 523]. Calculations were done on a 200-MHz personal computer and required approximately 75 s per iteration.
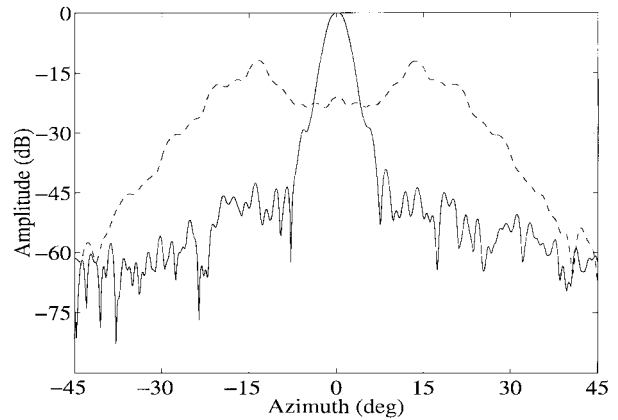
The second case was a more severe test

$$
\begin{pmatrix} \delta x \\ \delta y \\ \delta z \end{pmatrix} = \begin{pmatrix} 0.3 \cos(0.35n) \cos(0.65m) \\ 0.3 \cos(0.25n) \cos(0.15m) \\ \cos(0.15n) \cos(0.11m) \end{pmatrix} \lambda. \quad (11)
$$

The peak magnitude of this position error is 1.1λ and the rms magnitude is 0.52λ. Fig. 2 shows the result of probe position correction in this example. The pattern computed ignoring probe position errors bears little resemblance to the correct pattern—even the main beam is no longer recognizable. Again, there is no discernible difference between actual and position corrected patterns. For the displacements (11), the condition number is $c^2 \approx 21$, $\tau_9 < 10^{-4}$, and $\tau_{29} < 10^{-8}$.

In the third case we used position errors

$$
\begin{pmatrix} \delta x \\ \delta y \\ \delta z \end{pmatrix} = \begin{pmatrix} 0.3 \cos(0.35n + 4.55) \cos(0.65m + 4.2) \\ 0.3 \cos(0.25n - 4.25) \cos(0.15m + 2.85) \\ \cos(0.15n - 3.3) \cos(0.11m - 1.43) \end{pmatrix} \lambda
$$
$$(12)$$

which are similar to the second case but with phase offsets. This seems to be a minor change; nevertheless, the condition number increased to $c^2 \approx 490$ and 89 iterations were required to achieve a tolerance of 10^{-8} $(\tau_{89} < 10^{-8})$.

The reason for poor conditioning in the third case is the appearance of gaps (scallops) at the edges of the measurement area. In the fourth case we decreased L_x and L_y slightly to eliminate these gaps. Data falling outside the reduced boundaries were discarded. Also, it was advantageous to exclude data points lying within 0.1λ of the boundary. (Because of the periodic continuation of measurement space, data points too close to the boundary can result in excessive density there.) These changes reduced the condition number from $c^2 \approx 490$ to $c^2 \approx 42$ with $\tau_{37} < 10^{-8}$. (The total number of discarded data points was about 120 out of 26 000.)

The fifth case used the position errors of the second case [see (11)], but a phase gradient was introduced into the near-field data to steer the main beam $30°$ from boresight. As shown in Fig. 3 the pattern, ignoring probe position errors, bears little resemblance to the correct pattern. If we correct only
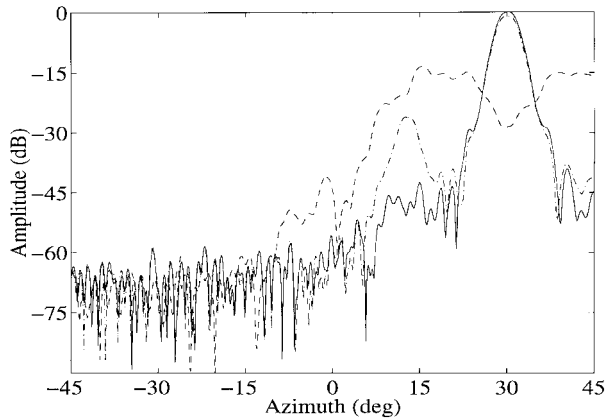
Fig. 3. *H*-plane far-field pattern of the radiometer with a steered beam. Probe position errors are given by (11). The solid line corresponds to the corrected pattern and to the actual pattern. The dashed line shows the result of ignoring the position errors. The dash-dotted line is the result of correcting only the *z*-position errors.
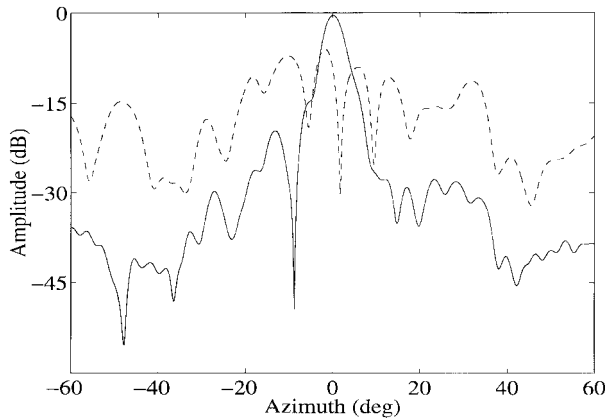

Fig. 4. *H*-plane far-field pattern of the dish (see Section V-B). The solid line corresponds to the pattern without position errors. The dashed line shows the result of ignoring the position errors.

for z position errors, much of the true pattern is recovered. However, the gain is still about 1 dB low, and there are anomalous sidelobes. The condition number and the number of iterations were the same as in the second case. This example demonstrates the importance of three-dimensional position error correction for steered-beam antennas.

B. Laboratory Tests

We want to verify that our method is effective in the presence of measurement errors. Three sets of near-field measurements were taken of a 1.2 m dish at 4 GHz. Two sets were made without position errors on planes separated by $\lambda/4$. In the third set, we deliberately introduced z-position errors (as a function of x). The errors included periodic and random components, and had a maximum magnitude of 0.5λ.

Results are shown in Figs. 4 and 5. From Fig. 4, we see that the position-error corrupted pattern is considerably distorted. Fig. 5 shows all three far-field patterns. Due to measurement errors (primarily multiple reflections), there are discrepancies. The patterns are consistent, however, within normal measurement uncertainties [10].
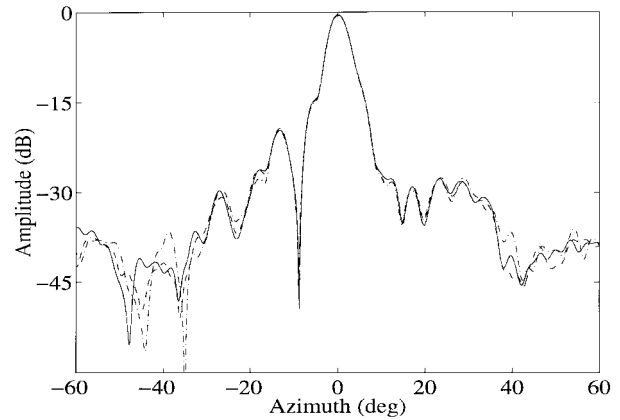

Fig. 5. *H*-plane far-field pattern of the dish (see Section V-B). The solid line corresponds to the pattern without position errors. The dashed line shows the pattern computed from data on the plane $z_0 + \lambda/4$, also without position errors. The dash-dotted line illustrates conjugate-gradient position-error correction.

C. Plane-Polar Grid

Beginning with the coupling product data of Section V-A, we simulated probe response on a plane-polar grid: maximum radius $r_{\max} = 43$ cm; radial step $\Delta r = 0.4\lambda$; angular step $\Delta\phi = \pi/356$ (so that $r_{\max}\Delta\phi = 0.4\lambda$). Data were retained within the rectangle $|x|$, $|y| < 30.59$ cm. In this setup, there are about 65 000 simulated measurements. A direct application of our algorithm resulted in a poor condition number $c^2 \approx 2$, 400, and $\tau_{100} \approx 5 \times 10^{-7}$.

The condition number can be dramatically reduced by finding a weighted least-squares solution of (2). For example, when data points were weighted by their measurement radii, the condition number was $c^2 \approx 46$ and $\tau_{29} < 10^{-8}$. This weighting scheme is consistent with an "information content" that is constant per unit area. Alternatively, when we simply thinned the data so that measurement spacing was never less than 0.15 cm, the condition number was reduced to $c^2 \approx 6$ and $\tau_{17} < 10^{-8}$. (In this setup, the number of simulated measurements is about 44 000.)

There are noniterative schemes for processing plane-polar data in $\mathcal{O}(N \log N)$ operations [11]–[15]. Our approach is more flexible, however, since data locations can be perturbed in three dimensions.

VI. SUMMARY

A number of papers treat nonideal measurement locations [16]–[23]. We think that our approach compares favorably in terms of efficiency, accuracy, and simplicity. Major features are:

- the algorithm is iterative, with a fixed cost per iteration that is $\mathcal{O}(N \log N)$. The memory requirement is $\mathcal{O}(N)$ and is independent of the number of iterations;
- convergence is guaranteed; bounds [see (6)] on the convergence rate for the conjugate gradient procedure are tighter than for many alternative iterative techniques;
- computation error (not measurement error) is bounded by the residual [see (7)];
- our current implementation is fully three dimensional;

- the recipe given in this paper is also applicable to cylindrical and spherical scanning geometries; the basic ingredient is an efficient procedure for predicting probe response at the measurement locations, based on an estimated modal spectrum.

Software implementing this method is available; interested readers should contact the authors.

APPENDIX A
PLANAR NEAR-FIELD SCANNING

Following Kerns [24], the response $w(\mathbf{r})$ of a receiving probe antenna (located at $\mathbf{r}$) to a transmitting test antenna (located at the origin) may be written as the Fourier transform

$$w(\mathbf{r}) = \int_{-\infty}^{\infty} \int_{-\infty}^{\infty} D(\mathbf{k}) \exp(i\mathbf{k} \cdot \mathbf{r}) \, dk_x \, dk_y \qquad (13)$$

where

$$\mathbf{k} = k_x \hat{\mathbf{x}} + k_y \hat{\mathbf{y}} + \gamma \hat{\mathbf{z}}$$
$$\gamma = k_z = \sqrt{k^2 - k_x^2 - k_y^2}$$
$$k \equiv \frac{2\pi}{\lambda}$$

and γ is chosen positive real or positive imaginary (the $\exp(-i\omega t)$ factor is suppressed). This model assumes that the probe is translated from place to place without rotation. The physical structures of the transmitting and receiving antennas must be entirely in the half spaces $z < 0$ and $z > 0$, respectively. Multiple interactions between antennas are ignored. Typically, we seek to determine coupling product $D(\mathbf{k})$ from measured values of $w(\mathbf{r})$.

Equation (13) is discretized by assuming, on some plane $z = d$, that $w(\mathbf{r}) = 0$ when $|x| \geq L_x$ or $|y| \geq L_y$. This approximation must be physically reasonable in the context of the measurement. The data then may be expressed as a Fourier series ($-L_x < x < L_x$, $-L_y < y < L_y$)

$$w(\mathbf{r}) = \sum_{\nu=-\infty}^{\infty} \sum_{\mu=-\infty}^{\infty} \xi_{\nu\mu} \exp(i\mathbf{k}_{\nu\mu} \cdot \mathbf{r}) \qquad (14)$$

with

$$\mathbf{k}_{\nu\mu} \equiv \frac{\pi\nu}{L_x} \hat{\mathbf{x}} + \frac{\pi\mu}{L_y} \hat{\mathbf{y}} + \gamma_{\nu\mu} \hat{\mathbf{z}}$$
$$\gamma_{\nu\mu} \equiv \sqrt{k^2 - \left(\frac{\pi\nu}{L_x}\right)^2 - \left(\frac{\pi\mu}{L_y}\right)^2}.$$

Now

$$\xi_{\nu\mu} = \frac{1}{4L_x L_y} \int_{-L_x}^{L_x} \int_{-L_y}^{L_y} w(\mathbf{r}) \exp(-i\mathbf{k}_{\nu\mu} \cdot \mathbf{r}) \, dx \, dy.$$

On the other hand, the Fourier transform (13) may be inverted to give

$$D(\mathbf{k}) = \frac{1}{4\pi^2} \int_{-L_x}^{L_x} \int_{-L_y}^{L_y} w(\mathbf{r}) \exp(-i\mathbf{k} \cdot \mathbf{r}) \, dx \, dy.$$

A comparison of the last two equations gives

$$\xi_{\nu\mu} = \frac{\pi^2}{L_x L_y} D(\mathbf{k}_{\nu\mu}). \qquad (15)$$

The infinite summation ranges in (14) must be truncated. A natural way to do this is to eliminate evanescent modes (γ imaginary). These usually contribute little to $w(\mathbf{r})$ since they are exponentially attenuated away from the transmitting antenna. For example, in standard planar near-field scanning applications, modal indices are limited by

$$-N_x \leq \nu < N_x, \quad -N_y \leq \mu < N_y \qquad (16)$$

where N_x and N_y are usually chosen just large enough to include all propagating modes

$$N_x \geq \frac{L_x}{\lambda/2}, \quad N_y \geq \frac{L_y}{\lambda/2}. \qquad (17)$$

With data $w(\mathbf{r}_{nm})$ measured on the grid

$$\mathbf{r}_{nm} = \frac{L_x n}{N_x} \hat{\mathbf{x}} + \frac{L_y m}{N_y} \hat{\mathbf{y}} + d\hat{\mathbf{z}} \qquad (18)$$

$$-N_x \leq n < N_x, \quad -N_y \leq m < N_y$$

(14) becomes a discrete Fourier transform. The FFT algorithm may be used to calculate the $\xi_{\nu\mu}$ in $\mathcal{O}(N \log N)$ operations ($N = 4N_x N_y$).

APPENDIX B
IMPLEMENTATION

According to the model (1) the coupling product $\boldsymbol{\xi} = \{\xi_{\nu\mu}\}$ is determined from the probe response $w(\mathbf{r})$ at a given set of measurement locations $\mathbf{r}_1, \cdots, \mathbf{r}_N$. As discussed above, there are fewer coefficients $\xi_{\nu\mu}$ than measurements (the problem is overdetermined), so the coefficients are found in a least-squares sense from the normal equations (3). The normal equations are solved iteratively using the conjugate gradient method.

This approach requires the repeated multiplication of the matrices $\mathbf{Q}$ and $\mathbf{Q}^H$ by vectors. The present method computes each matrix-vector product in $\mathcal{O}(N \log N)$ operations (for N measurements), in contrast to $\mathcal{O}(N^2)$ operations for evaluation by a direct method.

We first consider application of the matrix $\mathbf{Q}$. The measurement locations $\mathbf{r}_1, \cdots, \mathbf{r}_N$, with $\mathbf{r}_n = x_n \hat{\mathbf{x}} + y_n \hat{\mathbf{y}} + z_n \hat{\mathbf{z}}$, lie approximately on the plane $z = d$ and we assume that they are not more than a few wavelengths away from it. In particular, $|z_n - d| < a\lambda$ for $n = 1, \cdots, N$ with $a \lesssim 4$, where $\lambda = 2\pi/k$. This assumption allows the determination of $\exp(i\mathbf{k}_{\nu\mu} \cdot \mathbf{r}_n)$ by polynomial interpolation from a small set of values at fixed locations in z

$$\exp(i\mathbf{k}_{\nu\mu} \cdot \mathbf{r}_n) = \sum_{l=1}^{L} C_l(z_n) \exp(i\mathbf{k}_{\nu\mu} \cdot \mathbf{r}_{nl}) + \varepsilon_{\nu\mu n} \qquad (19)$$

where

$$\mathbf{r}_{nl} = x_n \hat{\mathbf{x}} + y_n \hat{\mathbf{y}} + \tilde{z}_l \hat{\mathbf{z}}$$
$$C_l(z_n) = \prod_{m=1, m \neq l}^{L} \frac{z_n - \tilde{z}_m}{\tilde{z}_l - \tilde{z}_m}$$

and the interpolation points are Chebyshev nodes defined by

$$\tilde{z}_l = \tilde{z}_0 + \frac{\tilde{z}_{L+1} - \tilde{z}_0}{2}\left[1 - \cos\frac{(2l-1)\pi}{2L}\right], \quad l = 1, \cdots, L$$
$$\tilde{z}_0 = \min_n z_n, \quad \tilde{z}_{L+1} = \max_n z_n. \tag{20}$$

The number L of interpolation nodes is chosen so the interpolation error $\varepsilon_{\nu\mu n}$ satisfies $|\varepsilon_{\nu\mu n}| < \varepsilon$, where ε is specified by the user. The polynomial interpolation error (see, for example, [25, p. 49]) is

$$\varepsilon_{\nu\mu n} = \prod_{l=1}^{L}(z_n - \tilde{z}_l) \cdot \frac{f^{(L)}(\zeta_{\mu n})}{L!}, \quad \zeta_{\mu n} \in [\tilde{z}_0, \tilde{z}_{L+1}]$$

where $f(z_n) = \exp(i\mathbf{k}_{\nu\mu} \cdot \mathbf{r}_n)$. For $\tilde{z}_1, \cdots, \tilde{z}_L$ defined by (20) and $|\gamma_{\nu\mu}| \leq k$, this reduces to the bound

$$|\varepsilon_{\nu\mu n}| \leq \frac{2(\pi a)^L}{L!}.$$

The smallest integer L such that $2(\pi a)^L/L! \leq \varepsilon$ therefore suffices.

Substituting (19) into (1) and changing the order of summation yields

$$w'(\mathbf{r}_n) = \sum_l C_l(z_n) \sum_{\nu\mu} \xi'_{\nu\mu} \exp(i\mathbf{k}_{\nu\mu} \cdot \mathbf{r}_{nl}) + \sum_{\nu\mu} \xi'_{\nu\mu} \varepsilon_{\nu\mu n}$$

where $\mathbf{w}' = \{w'(\mathbf{r}_n)\}$ is the probe response due to the coupling product $\boldsymbol{\xi}' = \{\xi'_{\nu\mu}\}$. The parameter ε is chosen so that the sum involving $\varepsilon_{\nu\mu n}$ can be neglected. The inner sum over $\nu\mu$ is a discrete Fourier transform in two dimensions for each l, except that the points $x_n\hat{\mathbf{x}} + y_n\hat{\mathbf{y}}$ are unequally spaced. The unequally spaced FFT of Dutt and Rokhlin [2] and, subsequently, Beylkin [3] can be used to evaluate this sum for all N locations in $\mathcal{O}(N \log N)$ operations. This evaluation is obtained for each of the planes $z = \tilde{z}_1, \cdots, \tilde{z}_L$ and the resulting values are weighted by the interpolation coefficients $C_l(z_n)$.

The multiplication of matrix $\mathbf{Q}^H$ by a vector is nearly the same as for $\mathbf{Q}$. The computation of $\mathbf{b}' \equiv \{b'_{\nu\mu}\}$ from $\mathbf{w}'$, where $\mathbf{b}' = \mathbf{Q}^H\mathbf{w}'$ is given by the equation

$$b'_{\nu\mu} = \sum_l C_l(z_n) \sum_n w'(\mathbf{r}_n) \exp(-i\mathbf{k}^*_{\nu\mu} \cdot \mathbf{r}_{nl}).$$

(Here, we have discarded the interpolation error term.) Again the inner sum is an unequally spaced Fourier transform in two dimensions for each l, except that the unequal spacing is over the summation index variable, rather than the free variable. Nevertheless, this case also requires $\mathcal{O}(N \log N)$ operations for each l.

Implementation of the unequally spaced FFT is rather elaborate; we use Beylkin's version which, for double-precision accuracy in two dimensions, requires roughly 25 times as much computation as a standard FFT of the same size. The overall cost of applying $\mathbf{Q}$ and $\mathbf{Q}^H$ depends on the deviation of the measurement locations from a plane and on the required accuracy. If, for example, $a = 0.5$ and $\varepsilon = 10^{-8}$, then $L = 15$ and each application of the matrix $\mathbf{A} = \mathbf{Q}^H\mathbf{Q}$ to a vector requires approximately $2 \cdot 15 \cdot 25 = 750$ times as much computation as a standard two-dimensional FFT. There

are a number of ways to reduce this constant, but it has been entirely adequate for our purposes.

The iterative solution of the normal equations (3) by the conjugate gradient method follows the procedure given in (5). In addition, we estimate the condition c^2 of the matrix $\mathbf{A}$ using the Lanczos method. This method exploits the connection between the condition of $\mathbf{A}$ and that of the Krylov matrices

$$\mathbf{K}(\mathbf{A}, \mathbf{r}^{(0)}, j) = [\mathbf{r}^{(0)}, \mathbf{A}\mathbf{r}^{(0)}, \cdots, \mathbf{A}^{j-1}\mathbf{r}^{(0)}], \quad j = 1, 2, \cdots$$

(see, for example, [6]). The method generates a sequence of symmetric tridiagonal matrices $\mathbf{T}_1, \mathbf{T}_2, \cdots$, with $\mathbf{T}_j$ of dimension $j \times j$, such that the extremal eigenvalues of $\mathbf{T}_j$ approximate those of $\mathbf{A}$ increasingly well. On the jth iteration of the conjugate gradient method, the estimate c_j^2 of the condition of $\mathbf{A}$ is obtained by diagonalizing $\mathbf{T}_j$ and defining $c_j^2 = \lambda_{j1}/\lambda_{jj}$, where $\lambda_{j1}, \lambda_{j2}, \cdots, \lambda_{jj}$ are the eigenvalues of $\mathbf{T}_j$ in descending order.

The matrix $\mathbf{T}_j$ is defined by the formula

$$\mathbf{T}_j = \begin{pmatrix} \alpha_0 & \beta_0 & \cdots & & 0 \\ \beta_0 & \alpha_1 & \ddots & & \vdots \\ \vdots & \ddots & \ddots & & \beta_{j-2} \\ 0 & \cdots & & \beta_{j-2} & \alpha_{j-1} \end{pmatrix}, \quad j = 1, 2, \cdots$$

where

$$\alpha_j = \frac{\|\mathbf{d}^{(j)}\|^2}{\|\mathbf{r}^{(j)}\|^2} + \frac{\|\mathbf{d}^{(j-1)}\|\|\mathbf{r}^{(j)}\|^2}{\|\mathbf{r}^{(j-1)}\|^4}$$
$$\beta_{j-1} = -\frac{\|\mathbf{d}^{(j-1)}\|^2\|\mathbf{r}^{(j)}\|}{\|\mathbf{r}^{(j-1)}\|^3}$$

for $j = 0, 1, \cdots$ and we define $\|\mathbf{r}^{(-1)}\| = 1$, $\|\mathbf{d}^{(-1)}\| = 0$.

The estimates c_j^2 of the condition of $\mathbf{A}$ are necessarily imperfect; they cannot account for aspects of $\mathbf{A}$ that are absent from $\mathbf{K}(\mathbf{A}, \mathbf{r}^{(0)}, j)$. These estimates, however, are best available given $\mathbf{K}(\mathbf{A}, \mathbf{r}^{(0)}, j)$. The Kaniel–Paige convergence theory (see [6]) establishes the connection between the estimates and the choice of $\boldsymbol{\xi}^{(0)}$.

REFERENCES

[1] R. C. Wittmann, B. K. Alpert, and M. H. Francis, "Planar near-field antenna measurements using nonideal measurement locations," in *Proc. Antenna Measurement Tech. Assoc.*, Seattle, WA, Sept. 30–Oct. 6, 1996, pp. 74–77.

[2] A. Dutt and V. Rokhlin, "Fast Fourier transforms for nonequispaced data," *SIAM J. Scientific Comput.*, vol. 14, pp. 1369–1393, Nov. 1993.

[3] G. Beylkin, "On the fast Fourier transform of functions with singularities," *Appl. Computat. Harmonic Anal.*, vol. 2, pp. 363–381, 1995.

[4] R. E. Kleinman and P. M. van den Berg, "Iterative methods for solving integral equations," in *PIER 5—Application of Conjugate Gradient Method to Electromagnetics and Signal Analysis*, T. K. Sarkar, Ed. New York: Elsevier, 1991, ch. 3.

[5] E. B. Joy and R. E. Wilson, "A simplified technique for probe position error compensation in planar surface near-field measurements," in *Proc. Antenna Measurement Techniques Assoc.*, Las Cruces, NM, Oct. 1982, pp. 14-1–14-10.

[6] G. H. Golub and C. F. Van Loan, *Matrix Computations*. Baltimore, MD: Johns Hopkins Univ. Press, 1989.

[7] S. Ponnapalli, "Near-field to far-field transformation utilizing the conjugate gradient method," in *PIER 5 Application of Conjugate Gradient Method to Electromagnetics and Signal Analysis*, T. K. Sarkar, Ed. New York: Elsevier, 1991, ch. 11.

[8] P. Petre and T. Sarkar, "Planar near-field to far-field transformation using an equivalent magnetic current approach," *IEEE Trans. Antennas Propagat.*, vol. 40, pp. 1348–1356, Nov. 1992.

[9] S. Blanch, R. G. Yaccarino, J. Rameu, and Y. Rahmat-Samii, "Near-field to far-field transformation of bipolar measurements by equivalent magnetic current approach," in *IEEE AP-S Int. Symp. Dig.*, Baltimore, MD, July 1996, vol. 1, pp. 561–564.

[10] A. C. Newell, "Error analysis techniques for planar near-field measurements," *IEEE Trans. Antennas Propagat.*, vol. 36, pp. 754–768, June 1988.

[11] O. M. Bucci, C. Gennarelli, and C. Savarese, "Fast and accurate near-field far-field transformation by sampling interpolation of plane-polar measurements," *IEEE Trans. Antennas Propagat.*, vol. 39, pp. 48–55, Jan. 1991.

[12] L. I. Williams, Y. Rahmat-Samii, and R. G. Yaccarino, "The bi-polar planar near-field measurement technique—Part I: Implementation and measurement comparisons," *IEEE Trans. Antennas Propagat.*, vol. 42, pp. 184–195, Feb. 1994.

[13] R. G. Yaccarino, Y. Rahmat-Samii, and L. I. Williams, "The bi-polar planar near-field measurement technique—Part II: Near-field to far-field transformation and holographic imaging methods," *IEEE Trans. Antennas Propagat.*, vol. 42, pp. 196–204, Feb. 1994.

[14] L. I. Williams, Y. Rahmat-Samii, and R. G. Yaccarino, "A comparison of polar, thinned-polar, and linear spiral sampling using the UCLA bi-polar planar near-field measurement system," in *Proc. Antenna Meas. Tech. Assoc.*, Williamsburg, VA, Nov. 1995, pp. 358–363.

[15] A. D. Yaghjian and M. B. Woodworth, "Sampling in plane-polar coordinates," *IEEE Trans. Antennas Propagat.*, vol. 44, pp. 696–700, May 1996.

[16] L. E. Corey, "Analytical compensation for near-field probe positioning errors in calculated far-field patterns," Ph.D. dissertation, Georgia Inst. Tech., Atlanta, May 1980.

[17] L. E. Corey and E. B. Joy, "On computation of electromagnetic fields on planar surfaces from fields on nearby surfaces," *IEEE Trans. Antennas Propagat.*, vol. AP-29, pp. 402–404, Mar. 1981.

[18] P. K. Agrawal, "A method to compensate for probe positioning errors in an antenna near-field facility," in *Proc. IEEE Antennas Propagat. Int. Symp.*, Albuquerque, NM, July 1982, pp. 218–221.

[19] L. A. Muth and R. L. Lewis, "A general technique to correct probe-position errors in planar near-field measurements to arbitrary accuracy," *IEEE Trans. Antennas Propagat.*, vol. 38, pp. 1925–1932, Dec. 1990.

[20] L. A. Muth, "General analytic correction for probe-position errors in spherical near-field measurements," *J. Res. Nat. Inst. Stand. Technol.*, vol. 96, pp. 391–410, July/Aug. 1991.

[21] L. A. Muth, "Probe-position error correction in planar near field measurements at 60 GHz: Experimental verification," *J. Res. Nat. Inst. Stand. Technol.*, vol. 97, pp. 273–297, Mar.–Apr. 1992.

[22] L. A. Muth, "General order N analytic correction of probe-position errors in planar near-field measurements," in *Proc. Antenna Measurement Tech. Assoc.*, Williamsburg, VA, Nov. 1995, pp. 331–335.

[23] M. H. Francis, "A comparison of k-correction and Taylor series correction for probe-position errors in planar near-field scanning," in *Proc. Antenna Measurement Tech. Assoc.*, Williamsburg, VA, Nov. 1995, pp. 341–347.

[24] D. M. Kerns, "Plane-wave scattering-matrix theory of antennas and antenna-antenna interaction," Nat. Bur. Stand. (U.S.) Monograph 162, 1981.

[25] J. Stoer and R. Bulirsch, *Introduction to Numerical Analysis.* New York: Springer-Verlag, 1980.

Ronald C. Wittmann (M'88–SM'98) received the B.S. degree from the University of Washington, Seattle, in 1972, and the M.S. degree in physics from the University of Colorado, Boulder, in 1976.

Since 1978, he has been employed by the Electromagnetic Fields Division, National Institute of Standards and Technology, Boulder, CO. His research interests are in remote sensing, near-field antenna measurements, and radar cross-section measurements.

Mr. Wittmann is a member of the IEEE Antenna Standards Committee.

Bradley K. Alpert received the B.S. degree from the University of Illinois, Urbana-Champaign, and the S.M. degree from University of Chicago, both in mathematics, in 1978 and 1979, respectively, and the Ph.D. degree in computer science from Yale University, New Haven, CT, in 1990.

He worked from 1979 to 1983 as a Casualty Actuary at CNA Insurance, Chicago, IL. He spent a postdoctoral year at University of California, Berkeley, Lawrence Berkeley Laboratory from 1990 to 1991 and joined National Institute of Standards and Technology (NIST), Boulder, CO, in 1991. His research interests include numerical solution of integral equations, fast transforms, high-order quadratures, and computational electromagnetics.

Michael H. Francis (M'82–SM'88) received the B.A. and the M.S. degrees in physics from the University of Colorado, Boulder, in 1973 and 1976, respectively.

From 1976 to 1980, he was a Research Assistant in the Department of Astrogeophysics at the University of Colorado, where he worked on modeling the solar atmosphere. Since 1980 he has been in the Electromagnetic Fields Division of the National Institute of Standards and Technology (NIST), where he works on antenna metrology problems. He has edited the *Antenna Measurement Techniques Association* (AMTA) *Newsletter* for the past seven years and is currently is the AMTA Technical Program Coordinator.

Mr. Francis is a member of the IEEE Antenna Standards Committee.